Equilibrium Point-based Control of Muscle-driven Endoskeleton: Modularity of Human Motor Control is applied to Control Anthropomorphic Legs

Journal:	*Advanced Robotics*
Manuscript ID	TADR-2018-0376
Manuscript Type:	Full paper
Date Submitted by the Author:	27-Dec-2018
Complete List of Authors:	Watanabe, Eichi; Osaka University, Department of Mechanical Science and Bioengineering Hirai, Hiroaki; Osaka University, Mechanical Science and Bioengineering Krebs, Hermano; Massachusetts Institute of Technology, Department of Mechanical Engineering
Keywords:	Biologically-Inspired Robots and Systems < System Design, and Integration, Humanoid Robots < System Design, and Integration
Manuscript Keywords:	musculoskeletal lower limb robot, muscle synergy, motor control, pedalling

Equilibrium Point-based Control of Muscle-driven Endoskeleton: Modularity of Human Motor Control is applied to Control Anthropomorphic Legs

Eichi Watanabe[a], Hiroaki Hirai[a] and Hermano Igo Krebs[b]

[a]*Department of Mechanical Science and Bioengineering, Graduate School of Engineering Science, Osaka University, Japan*

[b]*Department of Mechanical Engineering, Massachusetts Institute of Technology, Cambridge, USA*

E. Watanabe: watanabe@robotics.me.es.osaka-u.ac.jp

H. Hirai: hirai@me.es.osaka-u.ac.jp

H. I. Krebs: hikrebs@mit.edu

About the Authors

Eichi Watanabe joined Robotics and Mechatronics Laboratory in Department of Mechanical Science and Bioengineering, Osaka University, Japan from 2015. Currently, he is a PhD student at this laboratory and works on the research and development of rehabilitation robot for post stroke patients. He also had engaged in development of musculoskeletal lower limb robot. He holds a bachelor degree in Mechanical Engineering from Kanazawa University, Japan in 2015 and master degree in Mechanical Engineering from Osaka University, Japan in 2016. His current research interests are bio-inspired robotics and rehabilitation robotics. He is a Student Member of RSJ.

Hiroaki Hirai received B.E., M.E., and Ph. D degrees in Mechanical Engineering in 1997, 1999, and 2004, respectively, all from Osaka University, Japan. He is currently an Associate Professor (2016~) at Department of Mechanical Science and Bioengineering, Graduate School of Engineering Science, Osaka University. He is a co-inventor in the Osaka University-held patent on the muscle synergy analysis method, muscle synergy analyzer, and muscle synergy interface. He was a Visiting Researcher at the Eric P. and Evelyn E. Newman Laboratory for Biomechanics and Human Rehabilitation,

Department of Mechanical Engineering, Massachusetts Institute of Technology. He also worked at Yamaha Corporation as an engineer for electronic musical instruments. His current research interests include human motor control, human enhancement, and rehabilitation robotics.

Hermano Igo Krebs joined MIT's Mechanical Engineering Department in 1997 where he is a Principal Research Scientist and Lecturer – Newman Laboratory for Biomechanics and Human Rehabilitation. He also holds an affiliate position as an Adjunct Professor at University of Maryland School of Medicine, Department of Neurology, and as a Visiting Professor at Fujita Health University, Department of Physical Medicine and Rehabilitation, at University of Newcastle, Institute of Neuroscience, and at Osaka University, Department of Mechanical Engineering He is one of the founders and Chairman of the Board of Directors of Interactive Motion Technologies. He is a Fellow of the IEEE. Dr. Krebs was nominated by two of IEEE societies: IEEE-EMBS and IEEE-RAS to this distinguished engineering status "for contributions to rehabilitation robotics and the understanding of neuro-rehabilitation." Dr. Krebs has published and presented extensively on rehabilitation robotics. His work goes beyond Stroke and has been extended to Cerebral Palsy for which he received "The 2009 Isabelle and Leonard H. Goldenson Technology and Rehabilitation Award," from the Cerebral Palsy International Research Foundation (CPIRF). In 2015, he received the IEEE-INABA Technical Award for Innovation leading to Production "for contributions to medical technology innovation and translation into commercial applications for Rehabilitation Robotics." His goal is to revolutionize the way rehabilitation medicine is practiced today by applying robotics and information technology to assist, enhance, and quantify rehabilitation..

Equilibrium Point-based Control of Muscle-driven Endoskeleton: Modularity of Human Motor Control is applied to Control Anthropomorphic Legs

This study employs an approach that links the findings of robotics and neuroscience to propose a bio-inspired controlling method through musculoskeletal robot pedalling. It is attempted to control a musculoskeletal lower limb robot that imitates the human structure based on the framework of human motor control. Previous studies of pedalling have revealed that three pairs of biological functions in legs allow for forward and backward pedalling at a simulation level. This indicates that there is modularity of motor control between forward and backward pedalling. Equilibrium point (EP)-based synergies are introduced in our study to reveal the modularity of motor control from the point of stiffness and the end EP. Based on this, the findings of previous studies of pedalling are reinterpreted and applied to the analysis of human pedalling and the control of robots. The analysis results of EP-based synergy extracted from human subjects for forward and backward pedalling are in good agreement with previous studies. The musculoskeletal robot can achieve backward pedalling by modulating the EP-based synergies of forward pedalling. This result shows the potential of the bio-inspired control method in musculoskeletal robots based on the modularity of human motor control.

Keywords: musculoskeletal lower limb robot, muscle synergy, motor control, pedalling

1. Introduction

Humans can manage various kinds of movements flexibly and smoothly. In particular, the movements of the lower limb are sophisticated because of their dynamicity and the cooperation between two legs. Bipedal movement is realized by the musculoskeletal system and the control framework of multiple redundant structures. In the field of robotics, studies that focus on controlling musculoskeletal lower limb robots have been performed to determine the roles of the musculoskeletal system and establish a robotic structure that achieves flexible and smooth movements. The bipedal musculoskeletal robots that are activated by pneumatic muscles have achieved walking [1] and hopping [2]. Moreover, the robots that have biologically correct musculoskeletal structures have achieved running [3] and jumping [4]. Tendon-driven musculoskeletal robots have realized tricycle pedalling [5]. In the field of neuroscience, studies have investigated muscle synergies to reveal the framework of motor control in the human musculoskeletal structure. Muscle synergy is the hypothesis that focuses on the coordination of muscles. This coordination experiences the 'Bernstein Problem', which is the complexity of motor redundancy [6]. To verify this hypothesis, studies measured electromyograms (EMGs) and discussed the coordination of muscles. The studies that focused on lower limb motion (walking, running, pedalling, and so on) reported that there is an invariant structure in muscle coordination [7-12]. Studies in the fields of robotics and neuroscience have shown the roles and usability of the musculoskeletal structure and the framework of motor control in the lower limb. Comprehensive studies that employ an approach that links the findings of robotics and neuroscience are required for expanding the aforementioned studies. Moreover, such a bilateral approach might provide a new idea for establishing coordination between robots and humans. In recent years, the techniques that focus on robotics and neuroscience have been

investigated. A few pilot studies have controlled robots based on muscle synergies [13-18]. However, a few studies on muscle synergy discuss the lower limb. Thus, in this study, we focused on lower limb movement, i.e. pedalling, and proposed a biologically inspired control framework through muscle synergy analysis and robot control trials.

Pedalling is suitable task for the study of muscle coordination in the human body and for developing a musculoskeletal lower limb robot. The entire leg is under kinematical constraint during pedalling because of the structure of a bicycle. This restriction simplifies the redundancy of body structures. In addition, the continuous pumping of a pedal requires cooperation between the right and left legs via a crank. Based on this, the pedalling task is complex in terms of the force control required for cooperation between both legs. Thus, pedalling provides us a reasonable condition with kinematic constraints and dynamic interactions. Moreover, previous simulation studies on muscle coordination in human pedalling have clarified that six basic biological modules can be rearranged into three pairs, i.e. [Ext/Flex], [Ant/Post], and [Plant/Dorsi] [19-21]. There is no difference between forward and backward pedalling without the phase shifting of [Ant/Post] [20]. These studies provided concrete evidence on how muscle activity contributes to actual leg function and the modularity of motor function at a simulation level.

The present study proposes a bio-inspired control method based on EP-based synergy through a robotic and neuroscientific approach. The modularity of motor control in humans is discussed through EP-based synergies and applied to control a musculoskeletal lower limb robot. EP-based synergies, which are expressed by the composites of muscle mechanical impedance, are designed to clarify the modularity of motor control from the aspects of joint stiffness and the ankle EP. The formulation of the EP is based on the dynamical model of the lower limb. In this aspect, EP-based

synergies are different from muscle synergies, which are commonly discussed in neuroscience. As a result, in the EP-based synergy analysis, the synergy activation coefficient in the angular direction corresponding to the function of [Ant/Post] is shifted only in backward pedalling. In a control experiment, the musculoskeletal robot achieves backward pedalling with modified signals that are shifted based on a previous simulation report [20]. This study provides practical evidence for the control method based on EP-based synergies and the modularity of motor control.

2. Methods

The entire procedure of this study is shown in Figure 1. Experiments mainly consisted of two parts, i.e. human pedalling analysis and robot pedalling trials. The results from the two experiments are discussed to understand human motor control and confirm the usability of EP-based synergies for robot control.

2.1 Apparatus

2.1.1 Musculoskeletal lower limb robot

Structure. Figure 2 shows the musculoskeletal lower limb robot. The body parameters were determined from the database of human body parameters (Reference data: Japanese male, 18-23 y old) [22]. The details of the parameters are shown in Table I. Each leg was constructed to be similar to a human lower limb without mass. Mass was adjusted to be half of reference data because of actuator output power. Mass was adjusted by placing a lead plate on the surface of an anatomical model frame (3B Scientific GmbH, Germany). The positions of the centre of mass were also adjusted to coincide with reference data. As the motion of the lower limb on the sagittal plane is dominant during human pedalling, the degrees of freedom (DOFs) and motion were restricted on the sagittal plane. Each leg had three DOFs in the sagittal plane.

Actuator. The actuators were McKibben-type pneumatic artificial muscles (PAMs) (Kanda Tsushin Kogyo Co., Ltd., Japan). Each PAM was 2.54 cm in diameter, and its maximum contraction force was 800 N at a limit pressure 550 Pa. Eight PAMs were attached on the same location of the corresponding muscles in humans. The eight muscles were as follows: $M_{\mathrm{h,Ext}}$ (GM: gluteus maximus), $M_{\mathrm{h,Flex}}$ (ILIO: iliopsoas), $M_{\mathrm{hk,Ext}}$ (HAM: hamstring), $M_{\mathrm{hk,Flex}}$ (RF: rectus femoris), $M_{\mathrm{k,Ext}}$ (VM: vastus medialis),

$M_{k,Flex}$ (BF: biceps femoris), $M_{a,Ext}$ (GAS: gastrocnemius), and $M_{a,Flex}$ (TA: tibialis anterior). Suffixes 'h', 'hk', 'k', and 'a' indicate the hip, hip and knee, knee, and ankle, respectively. The robot contained 16 PAMs.

Control. Figure 3 shows the entire pneumatic circuit. Each PAM is connected to a custom-made air pressure controller (b) comprising an air pressure regulator (b1), a solenoid on–off valve (b2), and 16 servo valves (b3). Air is provided by a compressor and accumulator (a). The servo valves that are connected to a PC control the internal air pressure of the PAMs at a sampling rate of 1000 Hz. The commands for servo valves are determined based on the crank angle. Angle data are measured by an accelerometer (c1).

2.1.2 Customized bicycle

Figure 4 shows the customized bicycle. Human subjects and the robot perform pedalling on this device. The city-cycle style bicycle is used as the base frame. The back wheels are elevated by 3 cm by a metal frame structure. This frame contains an electromagnetic brake (ZA-1.2Y, Mitsubishi Electric Corp., Japan), extra sprockets, and a chain. The electromagnetic brake applies a constant brake torque on its crankshaft. The brakes are controlled by a PC via a single-board microcontroller (Arduino Uno SMD R3, Arduino S.R.L., Italia). The extra chain and sprockets connect the axles of the back wheels and a round-shaped deadweight. This structure prevents the slipping of the back wheel sprocket during backward pedalling. Similar to forward pedalling, subjects can feel resistance force during backward pedalling.

2.2 Analysis: EP-based synergies

2.2.1 Lower limb modelling

During pedalling, the movement of the lower limb is limited in the sagittal plane. The modelling is focused on the sagittal plane. Figure 5 shows the simplified structure of the human lower limb. This structure consists of three links and four pairs of eight muscles. Hereinafter, modelling is discussed based on this simplified structure. The four muscle pairs are the mono-articular muscle pairs around the hip, knee, and ankle joint and a bi-articular muscle pair between the hip and knee joint. The simplified structure is based on following assumptions: (1) A muscle can be assumed as a spring system whose elasticity and natural length are modulated according to the activation level of an EMG signal [23, 24]. (2) The contractile forces of the eight muscles are the same. (3) The lengths of the eight muscles are the same. (4) The moment arms, d, of each joint are the same, and they are constant regardless of the joint angle. (5) The lengths of the thigh and shank are the same.

2.2.2 Muscle modelling

Even though the biological muscle properties of PAMs are not identical to those of human muscles, assumption (1) is sufficient for developing a simple model of the complex musculoskeletal system. The input–output relationship of a PAM (inner pressure $P_{i,j}$ (i = h, hk, k, a, j = Ext, Flex) and contractile force) can be assumed to be equivalent to the input–output relationship of a biological muscle (EMG signal m and contractile force F) [23]. The contractile force of a PAM can be expressed as

$$F(P_{i,j}) = K(P_{i,j})(l_{i,j} - l_0(P_{i,j})) \quad (1)$$

where $K(P_{i,j})$ is the stiffness of the PAM at inner pressure P, $l_0(P_{i,j})$ is the natural length of the PAM at inner pressure P, and $l_{i,j}$ is the length of the PAM when it

contracts. Based on assumptions (2) and (3), this input–output model, i.e. Eq. (1), is the same for the eight muscles.

Constant coefficients are used to represent the properties of PAMs ($C_1 = 1.1 \times 10^2$ N, $C_2 = 9.6 \times 10^{-2}$ m, $C_3 = 1.2 \times 10^{-2}$ N/(mPa), and $C_4 = -1.8 \times 10^5$ Pa), and they are calculated from the mechanical property of PAMs [23]. $K(P_{i,j})$ and $l_0(P_{i,j})$ are given by

$$K(P_{i,j}) = C_3(P_{i,j} - C_4) = C_3\hat{P}_{i,j} \tag{2}$$

$$l_0(P_{i,j}) = C_1/K(P_{i,j}) + C_2 \tag{3}$$

2.2.3 Agonist–antagonist sums and agonist–antagonist ratios

The following parameters are introduced to examine the human motor strategy and control the musculoskeletal robot: (1) the ratio of the agonist–antagonist (A-A) muscle activity (A-A ratio) and (2) the sum of the A-A muscle activity (A-A sum). The first and second parameters are related to the equilibrium joint angle and joint stiffness, respectively.

The A-A sum, $s_i^{\mathrm{Rob}}(t)$, and A-A ratio, $r_i^{\mathrm{Rob}}(t)$, of the musculoskeletal robot are defined according to the inner pressure of the PAM, $\hat{P}_{i,j}(= P_{i,j} - C_4)$, as follows:

$$s_i^{\mathrm{Rob}}(t) = \hat{P}_{i,\mathrm{Ext}}(t) + \hat{P}_{i,\mathrm{Flex}}(t) \tag{4}$$

$$r_i^{\mathrm{Rob}}(t) = \hat{P}_{i,\mathrm{Ext}}(t)/(\hat{P}_{i,\mathrm{Ext}}(t) + \hat{P}_{i,\mathrm{Flex}}(t)) \tag{5}$$

where t is the measurement time. According to the presumed equivalency between the human musculoskeletal system and musculoskeletal robot system, the A-A sum, $s_i(t)$, and A-A ratio, $r_i(t)$, of humans are defined using the muscle activity of muscles, $m_{i,\mathrm{Ext}}(t)$ and $m_{i,\mathrm{Flex}}(t)$, as follows:

$$s_i(t) = m_{i,\mathrm{Ext}}(t) + m_{i,\mathrm{Flex}}(t) \tag{6}$$

$$r_i(t) = m_{i,\mathrm{Ext}}(t)/(m_{i,\mathrm{Ext}}(t) + m_{i,\mathrm{Flex}}(t)) \tag{7}$$

The functions of the A-A ratio and A-A sum are shown in Table II.

2.2.4 EP-based synergies

Ankle translation. Based on the statics in the lower limb, the displacement of the equilibrium joint angles of the hip, $\theta_{\mathrm{EP,h}}$, and knee, $\theta_{\mathrm{EP,k}}$, are approximated from Eqs. (1), (2), and (3) using r_i and s_i, as follows:

$$\begin{pmatrix}\theta_{\mathrm{EP,h}}\\ \theta_{\mathrm{EP,k}}\end{pmatrix} = C_5\begin{pmatrix}\boldsymbol{q}_1^T\\ \boldsymbol{q}_2^T\end{pmatrix}\begin{pmatrix}r_{\mathrm{h}} - \frac{1}{2}\\ r_{\mathrm{hk}} - \frac{1}{2}\\ r_{\mathrm{k}} - \frac{1}{2}\end{pmatrix} \tag{8}$$

$$\boldsymbol{q}_1 = \frac{-1}{s_{\mathrm{h}}s_{\mathrm{hk}} + s_{\mathrm{hk}}s_{\mathrm{k}} + s_{\mathrm{k}}s_{\mathrm{h}}}(s_{\mathrm{h}}s_{\mathrm{hk}} + s_{\mathrm{k}}s_{\mathrm{h}},\, s_{\mathrm{hk}}s_{\mathrm{k}},\, s_{\mathrm{hk}}s_{\mathrm{k}})^T \tag{9}$$

$$\boldsymbol{q}_2 = \frac{-1}{s_{\mathrm{h}}s_{\mathrm{hk}} + s_{\mathrm{hk}}s_{\mathrm{k}} + s_{\mathrm{k}}s_{\mathrm{h}}}(s_{\mathrm{h}}s_{\mathrm{hk}},\, -s_{\mathrm{h}}s_{\mathrm{hk}},\, s_{\mathrm{k}}s_{\mathrm{h}} + s_{\mathrm{hk}}s_{\mathrm{k}})^T \tag{10}$$

where $C_5(=1.78\ \mathrm{rad})$ is the coefficient determined by the muscle characteristics and moment arm of each joint. The detailed process for obtaining Eq. (8) is provided in the appendix. Under assumption (5), the ankle position in polar coordinates, $\boldsymbol{p}(t) = (R(t), \phi(t))^T$, is approximated from the joint angle, $(\theta_{\mathrm{h}}(t), \theta_{\mathrm{k}}(t))^T$, as follows:

$$\boldsymbol{p}(t) = \begin{pmatrix}R(t)\\ \phi(t)\end{pmatrix} = \begin{pmatrix}2L\cos(\frac{\theta_{\mathrm{k}}(t)}{2})\\ \theta_{\mathrm{h}}(t) - \theta_{\mathrm{k}}(t)\end{pmatrix} \tag{11}$$

where L is the mean length of the thigh and shank. Based on this relationship and ($\boldsymbol{q}_1$, $\boldsymbol{q}_2$), which is assumed to be constant about the EP, $\Delta\boldsymbol{p}_{\mathrm{EP}} = (\Delta R, \Delta\phi)$ can be expressed as follows:

$$\Delta \boldsymbol{p}_{\mathrm{EP}}(t) = \begin{pmatrix} \Delta R(t) \\ \Delta \phi(t) \end{pmatrix}$$

$$= C_5 \begin{pmatrix} 0 & -L\sin(\bar{\theta}_k(t)/2) \\ 1 & -1/2 \end{pmatrix} \begin{pmatrix} \Delta\theta_{\mathrm{EP,h}}(t) \\ \Delta\theta_{\mathrm{EP,k}}(t) \end{pmatrix}$$

$$= \begin{pmatrix} C_6 & 0 \\ 0 & C_7 \end{pmatrix} \begin{pmatrix} \boldsymbol{q}_2^T \\ (\boldsymbol{q}_1 - \boldsymbol{q}_2)^T \end{pmatrix} \begin{pmatrix} \Delta r_{\mathrm{h}}(t) \\ \Delta r_{\mathrm{hk}}(t) \\ \Delta r_{\mathrm{k}}(t) \end{pmatrix} \qquad (12)$$

Here, constants $C_6 (= -0.44$ m) and $C_7 (= 0.67$ rad) are given by the characteristics of the muscle, the length of the link, and moment arms.

The base vectors of the movement of the ankle EP in the radial and angular directions, or the reference frame in the muscle space for the ankle position, are determined by A-A sums.

$$\mathbf{u}_R = \boldsymbol{q}_2/|\boldsymbol{q}_2| \qquad (13)$$

$$\mathbf{u}_\phi = (\boldsymbol{q}_1 - \boldsymbol{q}_2/2)/|\boldsymbol{q}_1 - \boldsymbol{q}_2/2| \qquad (14)$$

$\mathbf{u}_R$ and $\mathbf{u}_\phi$ are defined as the muscle synergy vectors in the radial and angular directions, respectively. Here, $\mathbf{u}_R$ and $\mathbf{u}_\phi$ are the basis of the translational displacement of the ankle EP in the polar coordinate system. The linear combination of the synergy vectors under polar coordinates provides the displacement of the ankle EP. The displacement of A-A ratios in the synergy space is analysed to discuss a virtual trajectory. The displacement of A-A ratios, $\Delta \boldsymbol{r} = (r_{\mathrm{h}}(t) - \bar{r}_{\mathrm{h}}\ , r_{\mathrm{hk}}(t) - \bar{r}_{\mathrm{hk}}\ , r_{\mathrm{k}}(t) - \bar{r}_{\mathrm{k}}\ )^T$, is projected on the coordinate plane that is defined by the synergy vectors, as follows:

$$\begin{pmatrix} \Delta w_R(t) \\ \Delta w_\phi(t) \end{pmatrix} = \begin{pmatrix} \mathbf{u}_R^T \\ \mathbf{u}_\phi^T \end{pmatrix} \begin{pmatrix} \Delta r_{\mathrm{h}}(t) \\ \Delta r_{\mathrm{hk}}(t) \\ \Delta r_{\mathrm{k}}(t) \end{pmatrix} \qquad (15)$$

$\Delta w_R(t)$ and $\Delta w_\phi(t)$ are the synergy activation coefficients in the radial and angular directions, respectively. These coefficients have the following proportional relationships:

$$\Delta R(t) \propto \Delta w_R(t) \tag{16}$$

$$\Delta \phi(t) \propto \Delta w_\phi(t) \tag{17}$$

In this study, we discussed the synergy activation coefficients as the virtual trajectory.

Ankle rotation. The ankle EP angle is calculated according to the A-A ratio, r_{a}, and A-A sum, $\mathrm{s_a}$. The rotational displacement of the ankle EP angle, $\theta_{\mathrm{EP,a}}$, is expressed as follows:

$$\theta_{\mathrm{EP,a}}(t) = C_8 r_{\mathrm{a}}(t) \tag{18}$$

where C_8 is the constant coefficient that converts the A-A ratio, r_{a}, to the displacement of the ankle EP angle. In this study, r_{a} is considered to be the same as $\theta_{\mathrm{EP,a}}$. The stiffness that affects the ankle EP angle is evaluated from the A-A sum of the ankle, $\mathrm{s_a}$. The process of the formulation of EP-based synergy is described in our previous study [25].

2.2.5 Interpretation of EP-based synergies

The simulation-based studies of human pedalling have revealed that pedalling is enabled by three main biological pairs, i.e. [Ext/Flex], [Ant/Post], and [Plant/Dorsi] [19-21]. We assume that these three functions correspond to the function of our EP-based synergies. Figure 6 shows the one-to-one correspondence of the functions between simulation-based analysis and EP-based synergy analysis. The translation of the ankle EP includes the function of [Ext/Flex] and [Ant/Post]. The direction of [Ext/Flex]

coincides with radial synergy vector $\mathbf{u}_R$. When the synergy activation coefficient in the radial direction, Δw_R, becomes more than or less than zero, the ankle EP becomes [Ext] or [Flex.] The direction of [Ant/Post] coincides with angular synergy vector $\mathbf{u}_\phi$. When the synergy activation coefficient in the angular direction, Δw_ϕ, becomes more than or less than zero, the ankle EP becomes [Ant] or [Post]. The rotation of the ankle EP includes the function of [Plant/Dorsi]. The direction of [Plant/Dorsi] coincides with the A-A ratio of the ankle, r_{a}, which is related to equilibrium angle of the ankle. When the value of r_{a} becomes close to 1.0 or 0, the ankle joint becomes [Plant] or [Dorsi].

Ting et al. found that humans could achieve forward and backward pedalling based on the same biological functions, i.e. [Ext/Flex], [Ant/Post], and [Plant/Dorsi] [20]. Additionally, there is only an [Ant/Post] phase shift of 50% between forward and backward pedalling by humans (Figure 3). The other functions are not shifted. Based on these findings, the concept of EP-based synergy can be rewritten as follows: only the synergy activation coefficient (virtual trajectory) in the angular direction, Δw_ϕ, is shifted by 180° between forward and backward pedalling.

2.3 Implementation: Control commands for robot

The commands for the PAMs are calculated based on human EP-based synergies. This chapter shows the procedure of the implementation in the musculoskeletal robot through human EP-based synergy extraction by considering the phase reversal discussed in the simulation study [20] (Figure 7).

2.3.1 A-A sum and A-A ratio for ankle translation

The A-A sum of the robot, $\boldsymbol{s}^{\mathrm{Rob}}(\psi) = (s_{\mathrm{h}}^{\mathrm{Rob}}(\psi), s_{\mathrm{hk}}^{\mathrm{Rob}}(\psi), s_{\mathrm{k}}^{\mathrm{Rob}}(\psi))$, is determined based on the A-A sum of human subjects, $\boldsymbol{s}^{\mathrm{Hum}}(\psi)$.

$$\boldsymbol{s}^{\mathrm{Rob}}(\psi - \alpha) = \boldsymbol{s}^{\mathrm{Hum}}(-\psi) \tag{19}$$

where ψ is the magnitude of the crank angle during one pedalling phase ($0° \leqq \psi \leqq 360°$). The rotation of crank is reversed for backward pedalling. Thus, the commands are reversed to $-\psi$. α is the parameter that compensates for time delays in the system, e.g. the delay in the air pressure control device ($\alpha = 30 \pm 10°$).

The A-A ratio of the robot, $\boldsymbol{r}^{\mathrm{Rob}}(\psi) = \left(r_{\mathrm{h}}^{\mathrm{Rob}}(\psi), r_{\mathrm{hk}}^{\mathrm{Rob}}(\psi), r_{\mathrm{k}}^{\mathrm{Rob}}(\psi)\right)$, is determined based on the synergy vectors, $\mathbf{u}_R$ and $\mathbf{u}_\phi$, and synergy activation coefficients, Δw_R and w_ϕ, of human subjects. Based on the simulation study [20], the phase of the synergy activation coefficient in the angular direction, Δw_ϕ, which coincides with [Ant/Post] in the simulation, is shifted by 180° to achieve backward pedalling. The A-A ratios of ankle translation are as follows:

$$\boldsymbol{r}^{\mathrm{Rob}}(\psi - \alpha) = \Delta w_R(-\psi)\mathbf{u}_R + \Delta w_\phi(180 - \psi)\mathbf{u}_\phi + \bar{\boldsymbol{r}}^{\mathrm{Rob}} \tag{20}$$

$\bar{\boldsymbol{r}}^{\mathrm{Rob}}$ is determined based on the A-A ratio of one pedalling phase, $\boldsymbol{r}^{\mathrm{Hum}}(\psi)$. There are mechanical and structural differences between humans and the musculoskeletal robot. $\bar{\boldsymbol{r}}^{\mathrm{Rob}}$ is experimentally determined to minimize these differences.

2.3.2 A-A sum and A-A ratio for ankle rotation

The A-A sum and A-A ratio of the ankle of the robot, $s_{\mathrm{a}}^{\mathrm{Rob}}(\psi)$ and $r_{\mathrm{a}}^{\mathrm{Rob}}(\psi)$, are directly determined from those of human subjects.

$$s_{\mathrm{a}}^{\mathrm{Rob}}(\psi-\alpha)=s_{\mathrm{a}}^{\mathrm{Hum}}(-\psi) \tag{21}$$

$$r_{\mathrm{a}}^{\mathrm{Rob}}(\psi-\alpha)=r_{\mathrm{a}}^{\mathrm{Hum}}(-\psi) \tag{22}$$

2.3.3 Pressure commands for PAMs

The pressure commands for PAMs are calculated based on Eqs. (4) and (5). The commands for right-side PAMs, $P_{i,j}(\psi)$, $(j=\mathrm{Ext,\ Flex})$, are as follows:

$$P_{i,\mathrm{Flex}}(\psi)=k_p(1-r_i^{\mathrm{Rob}}(\psi))s_i^{\mathrm{Rob}}(\psi) \tag{23}$$

$$P_{i,\mathrm{EXT}}(\psi)=k_p r_i^{\mathrm{Rob}}(\psi)s_i^{\mathrm{Rob}}(\psi) \quad (i=\mathrm{h,hk,k,a}) \tag{24}$$

k_p is the gain constant used to tune the pressure commands based on the limit of the PAMs. The commands for the left-side leg are obtained by shifting the data of the right-side leg by 180°.

2.4 Measurement of human pedalling

2.4.1 Subjects

Five healthy subjects volunteered (all male; 22.8±1.71 y old; 1.69±0.034 m; 60.8±7.27 kg). These subjects were daily users of the city-cycle style bicycle. The subjects provided informed consent, and the Institutional Review Board of Osaka University approved the presented procedures. The tasks were forward and backward pedalling at 60 rpm under a constant torque burden of 30 Nm.

2.4.2 Protocol

The experimental setup is shown in Figure 8. Five subjects were asked to ride and pedal as usual. The positions of the hip (height of saddle) and foot (contact point of pedal) were determined by every subject with comfortability. Before the measurement, the subjects were instructed to pedal forward and backward at a constant cadence of 60 rpm, which was measured by a digital metronome (MA1RD, KORG INC, Japan). After the instruction, the metronome was turned off and measurement was started for 30 s. EMGs were recorded by a multi-telemeter system (WEB-5000, Nihon Kohden Corp., Japan) from the electrodes that were attached on the surface above the target muscles. Before attaching the electrodes, the skin was cleaned using medical alcohol to decrease impedance to under 30 kΩ. The recorded EMGs were analysed after bandpass filtering (20 to 450 Hz), full-wave rectification, smoothing, and normalization to maximum voluntary contraction (%MVC). The kinematics of the hip, knee, ankle, and crank angle were recorded by a tracking camera (OptiTrack, NaturalPoint Inc., USA). The pedalling force of the right foot was measured by a triaxial force sensor (M3D, Tech Gihan Co., Ltd., Japan). The EMGs, kinematics, and pedalling force were synchronized at 100 Hz.

3. Results

3.1 EP-based synergies

Figure 9 shows the averaged EP-based synergies obtained from the five subjects. The upper and lower parts show the results of forward and backward pedalling, respectively. The results are categorized into two functions, i.e. ankle translation and rotation.

3.1.1 Ankle translation (Ext/Flex) (Ant/Post)

In the bar graphs (RGB coloured) shown in Figure 9, the bars on the right and left sides show the EP-based synergy vectors in the radial and angular directions, $\mathbf{u}_R$ and $\mathbf{u}_\phi$, respectively. $\mathbf{u}_R$ and $\mathbf{u}_\phi$ denote the activation balance of A-A muscle pairs in the radial [Ext/Flex] and angular [Ant/Post] directions, respectively. In these bar graphs, the left (red), middle (green), and right (blue) bars represent the A-A muscle activation of the (1) hip joint, (2) hip and knee joint, and (3) knee joint, respectively. If the value becomes close to 1.0 or -1.0, the joint is under extension or flexion. The dots-and-line graphs in Figure 9 show the synergy activation coefficient (virtual trajectory) of the right leg. The shaded area shows the standard deviation among the five subjects. The dots are plotted in the 5% pedalling phase interval.

3.1.2 Ankle rotation (Plant/Dorsi)

The right column of Figure 9 shows the A-A ratio and A-A sum of the ankle during forward and backward pedalling. The upper and lower parts show the results of forward and backward pedalling, respectively. The shaded area shows the standard deviation among the five subjects.

3.2 Robot trial

The musculoskeletal lower limb robot could achieve backward pedalling based on the modified commands of forward pedalling provided in Ting's report [20]. Even though the cadence of the robot was slower than that of human subjects, backward pedalling

was performed smoothly. Figure 10 shows the sequential photographs of every quarter of the pedalling cycle phase. The solid and dotted arrows represent the magnitude and direction of the total pedalling force of the robot and humans, respectively. The ankle positions in panels (A)–(E) are almost 0°, 90°, 180°, and 270°, indicating that the robot reproduces constant pedal speed.

4. Discussion

4.1 EP-based synergies

4.1.1 Ankle translation (Ext/Flex) (Ant/Post)

EP-based synergy vectors. According to the bar graphs shown in Figure 9, the vectors of forward and backward pedalling are similar. The inner products between $\mathbf{u}_R$ or $\mathbf{u}_\phi$ for forward and backward pedalling are 0.93 ± 0.04. These results confirm that the balance of muscle mechanical impedance has an invariant structure. The five subjects are daily users of bicycles; hence, they are not used to backward pedalling. This implies that the EP-based synergy vectors, which represent muscle activation patterns, are invariant regardless of the skill level of the five subjects for the tasks.

Synergy activation coefficients (Virtual trajectory). According to the dots-and-line graphs shown in Figure 9, the synergy activation coefficients consistently precede the actual ankle position for approximately 50% of one pedalling phase. This preceding transition of the EP from the actual position indicates that the muscle activation that contributes to ankle translation is planned in advance for generating force to push the pedal. The phase of the EP trajectory between forward and backward pedalling is almost reversed. This implies that the phase of Δw_ϕ corresponding to the function of [Ant/Post] is almost shifted by 180°. This result coincides with the simulation study [20].

Moreover, the activation coefficients describe the characteristics of forward and backward pedalling. The trajectories of forward pedalling are more circular than those of backward pedalling. Even though the EP-based synergy vectors are almost identical between forward and backward pedalling, the activation coefficients are unique in both

cases. Considering this point, the synergy activation coefficient is a critical factor that characterizes the motor strategy of the five subjects.

4.1.2 Ankle rotation (Plant/Dorsi)

According to the A-A ratio shown in Figure 9, a common trend that ankle rotation becomes plantar flexion is observed for forward and backward pedalling during the push-down phase in the pedalling cycle. Based on the A-A sum shown in Figure 9, the stiffness of the A-A muscle during the push-down phase becomes higher compared to the pull-up phase in forward and backward pedalling. Regardless of rotation direction, the phase from 0% to 50% is important for transmitting pedalling force to the crank. Thus, the ankle is plantar flexed and has higher stiffness during this phase. The phase of r_a is the same or slightly (approximately 10%) shifted between forward and backward pedalling. This is in agreement with simulation studies [18-20].

4.2 Robot trial

The robot performs smooth backward pedalling at a cadence of approximately 30 rpm. The magnitude of the pedalling force of the robot is approximately one-fifth of that of human subjects. Considering the energy conservation law, the rotational speed of the crank is $\omega_{crank} = \sqrt{4\overline{F}_p\pi/(mR)}$, where $\overline{F}_p$ is the average pedalling force, m is the weight of the legs, and R is the length of the crank. The crank rotational speed is a multiple of $2/\sqrt{10}(\simeq 0.63)$. It is equal to the original human pedalling speed when the value of $\overline{F}_p$ is $1/5$ and the value of m is half of the weight of a human subject. This estimation is slightly different from the robot pedalling cadence obtained from the experiment. The number of muscles may be related to this difference. In this study, we focused on eight muscles (four A-A muscle pairs) for EP-based synergies. However, the actual human body is activated by numerous muscles. This difference affects the small gap in force output. Therefore, the result that the musculoskeletal robot achieves

backward pedalling based on the function of forward pedalling supports the simulation study [20].

By introducing EP-based synergies from the five subjects, the robot generates different pedalling that emphasizes the characteristic of each subject. The ankle trajectories and cadence of the human subjects are the same because of the constraint of pedalling. However, the output force (direction and magnitude), cadence, and ankle angle are different in the reproduction by the robot. This implies that EP-based synergies have the ability to depict the characteristics of the tasks performed by individual subjects.

5. Conclusion

EP-based synergies clarified the characteristics of forward and backward pedalling at the muscle activity level. The results obtained through EP-based synergy coincided with the results obtained from previous simulation studies [18-20]. The phase reversal of the [Ant/Post] function, i.e. the synergy activation coefficient in the angular direction, occurred between forward and backward pedalling. This showed the modularity between forward and backward pedalling. Moreover, EP-based synergies revealed the following characteristics: The balance of muscle mechanical impedance, i.e. synergy vectors, extracted from human pedalling was similar between forward and backward pedalling. This showed that humans have a common and invariant structure of mechanical impedance. Considering the fact that backward pedalling is an unfamiliar task for humans, we can speculate that mechanical impedance is invariant regardless of whether humans are well skilled in the task of backward pedalling or not. The synergy activation coefficients related to the virtual trajectory described the detail of the characteristics of forward and backward pedalling. The transition speed and path shape of the ankle EP (synergy activation coefficients) had a unique pattern in forward and backward pedalling.

The musculoskeletal robot achieved backward pedalling based on the EP-based synergies of forward pedalling. This showed the usability of EP-based synergy for controlling the musculoskeletal robot. The commands of backward pedalling were generated from the EP-based synergies of forward pedalling based on the simulation study [20]. There was no phase shift of [Ant/Post] between forward and backward pedalling. This result coincided with the simulation study [20] and EP-based synergy analysis. Moreover, it demonstrated the modularity of motor function. This indicates

that human motor control command could be a useful tool for controlling musculoskeletal robots.

In conclusion, the results reported in this paper provide evidence for (1) the usability of EP-based synergies in muscle coordination analysis and (2) the potential of EP-based synergies and the motor control of human pedalling for controlling musculoskeletal robots.

6. Appendix

The process from lower limb statics to EP-based synergies is described below.

For the ankle translation EP, the equilibrium relationships between the forces and geometry of PAMs are given by assumptions (2), (3), and (4).

Forces of PAMs

$$F(P_{\mathrm{h,Ext}}) - F(P_{\mathrm{h,Flex}}) + F(P_{\mathrm{hk,Ext}}) - F(P_{\mathrm{hk,Flex}}) = 0 \quad \text{(x1)}$$

$$-F(P_{\mathrm{hk,Ext}}) + F(P_{\mathrm{hk,Flex}}) + F(P_{\mathrm{k,Ext}}) - F(P_{\mathrm{k,Flex}}) = 0 \quad \text{(x2)}$$

Geometry of PAMs

$$d\theta_{\mathrm{h}} = l_{\mathrm{h,Ext}} - l_{\mathrm{EP}}(P_{\mathrm{h,Ext}}) = l_{\mathrm{EP}}(P_{\mathrm{h,Flex}}) - l_{\mathrm{h,Flex}} \quad \text{(x3)}$$

$$d(\theta_{\mathrm{h}} - \theta_{\mathrm{k}}) = l_{\mathrm{hk,Ext}} - l_{\mathrm{EP}}(P_{\mathrm{hk,Ext}}) = l_{\mathrm{EP}}(P_{\mathrm{hk,Flex}}) - l_{\mathrm{hk,Flex}} \quad \text{(x4)}$$

$$d\theta_{\mathrm{k}} = l_{\mathrm{k,Ext}} - l_{\mathrm{EP}}(P_{\mathrm{k,Ext}}) = l_{\mathrm{EP}}(P_{\mathrm{k,Flex}}) - l_{\mathrm{k,Flex}} \quad \text{(x5)}$$

$l_{\mathrm{EP}}(P_{i,j})$ denotes the length of the EP of the force of the PAM, and d is the radius of each joint. Eq. (3) can be arranged as the following relationship between the EP joint angles, $\theta_{\mathrm{EP,h}}$ and $\theta_{\mathrm{EP,k}}$, based on Eqs. (x3)–(x5) and assumption (5):

$$\begin{pmatrix} K(P_{\mathrm{h,Ext}}) + K(P_{\mathrm{h,Flex}}) + K(P_{\mathrm{hk,Ext}}) + K(P_{\mathrm{hk,Flex}}) & -(K(P_{\mathrm{hk,Ext}}) + K(P_{\mathrm{hk,Flex}})) \\ -(K(P_{\mathrm{hk,Ext}}) + K(P_{\mathrm{hk,Flex}})) & K(P_{\mathrm{hk,Ext}}) + K(P_{\mathrm{hk,Flex}}) + K(P_{\mathrm{k,Ext}}) + K(P_{\mathrm{k,Flex}}) \end{pmatrix} \begin{pmatrix} \theta_{\mathrm{EP,h}} \\ \theta_{\mathrm{EP,k}} \end{pmatrix}$$

$$= \frac{l_0(P_{i,j}) - C_2}{d} \begin{pmatrix} P_{\mathrm{h,Ext}} - P_{\mathrm{h,Flex}} + P_{\mathrm{hk,Ext}} - P_{\mathrm{hk,Flex}} \\ -(P_{\mathrm{hk,Ext}} - P_{\mathrm{hk,Flex}} - P_{\mathrm{k,Ext}} + P_{\mathrm{k,Flex}}) \end{pmatrix} \quad \text{(x6)}$$

The relationships between the EP joint angles and PAMs are expressed as follows based on Eq. (2):

$$\begin{pmatrix} \hat{P}_{\mathrm{h,Ext}} + \hat{P}_{\mathrm{h,Flex}} + \hat{P}_{\mathrm{hk,Ext}} + \hat{P}_{\mathrm{hk,Flex}} & -(\hat{P}_{\mathrm{hk,Ext}} + \hat{P}_{\mathrm{hk,Flex}}) \\ -(\hat{P}_{\mathrm{hk,Ext}} + \hat{P}_{\mathrm{hk,Flex}}) & \hat{P}_{\mathrm{hk,Ext}} + \hat{P}_{\mathrm{hk,Flex}} + \hat{P}_{\mathrm{k,Ext}} + \hat{P}_{\mathrm{k,Flex}} \end{pmatrix} \begin{pmatrix} \theta_{\mathrm{EP,h}} \\ \theta_{\mathrm{EP,k}} \end{pmatrix}$$

$$= \frac{l_0(P_{i,j}) - C_2}{d}\begin{pmatrix} \hat{P}_{\mathrm{h,Ext}} - \hat{P}_{\mathrm{h,Flex}} + \hat{P}_{\mathrm{hk,Ext}} - \hat{P}_{\mathrm{hk,Flex}} \\ -(\hat{P}_{\mathrm{hk,Ext}} - \hat{P}_{\mathrm{hk,Flex}} - \hat{P}_{\mathrm{k,Ext}} + \hat{P}_{\mathrm{k,Flex}}) \end{pmatrix} \quad \text{(x7)}$$

Eq. (x7) can be modified as follows based on the A-A ratio ($r_i = \hat{P}_{i,\mathrm{Ext}}/(\hat{P}_{i,\mathrm{Ext}} + \hat{P}_{i,\mathrm{Flex}})$) and A-A sum ($s_i = \hat{P}_{i,\mathrm{Ext}} + \hat{P}_{i,\mathrm{Flex}}$):

$$\begin{pmatrix} s_{\mathrm{h}} + s_{\mathrm{hk}} & -s_{\mathrm{hk}} \\ -s_{\mathrm{hk}} & s_{\mathrm{hk}} + s_{\mathrm{k}} \end{pmatrix}\begin{pmatrix} \theta_{\mathrm{EP,h}} \\ \theta_{\mathrm{EP,k}} \end{pmatrix} = \frac{l_0 - C_2}{d}\begin{pmatrix} A + B \\ -(B - C) \end{pmatrix} \quad \text{(x8)}$$

A, B, and C are expressed as follows:

$$A = 2(\hat{P}_{\mathrm{h,Ext}} + \hat{P}_{\mathrm{h,Flex}})\left(\frac{\hat{P}_{\mathrm{h,Ext}}}{\hat{P}_{\mathrm{h,Ext}} + \hat{P}_{\mathrm{h,Flex}}} - \frac{1}{2}\right) = \mathrm{s_h}(r_{\mathrm{h}} - 1/2) \quad \text{(x9)}$$

$$B = 2(\hat{P}_{\mathrm{hk,Ext}} + \hat{P}_{\mathrm{h,Flex}})\left(\frac{\hat{P}_{\mathrm{hk,Ext}}}{\hat{P}_{\mathrm{hk,Ext}} + \hat{P}_{\mathrm{hk,Flex}}} - \frac{1}{2}\right) = \mathrm{s_{hk}}(r_{\mathrm{hk}} - 1/2) \quad \text{(x10)}$$

$$C = 2(\hat{P}_{\mathrm{k,Ext}} + \hat{P}_{\mathrm{k,Flex}})\left(\frac{\hat{P}_{\mathrm{k,Ext}}}{\hat{P}_{\mathrm{k,Ext}} + \hat{P}_{\mathrm{k,Flex}}} - \frac{1}{2}\right) = \mathrm{s_k}(r_{\mathrm{k}} - 1/2) \quad \text{(x11)}$$

Eq. (x8) can be rewritten as follows:

$$\begin{pmatrix} s_{\mathrm{h}} + s_{\mathrm{hk}} & -s_{\mathrm{hk}} \\ -s_{\mathrm{hk}} & s_{\mathrm{hk}} + s_{\mathrm{k}} \end{pmatrix}\begin{pmatrix} \theta_{\mathrm{EP,h}} \\ \theta_{\mathrm{EP,k}} \end{pmatrix} = \frac{2(l_0 - C_2)}{d}\begin{pmatrix} \mathrm{s_h}(r_{\mathrm{h}} - 1/2) + \mathrm{s_{hk}}(r_{\mathrm{hk}} - 1/2) \\ -(\mathrm{s_{hk}}(r_{\mathrm{hk}} - 1/2) - \mathrm{s_k}(r_{\mathrm{k}} - 1/2)) \end{pmatrix}$$

$$= \frac{2(l_0 - C_2)}{d}\begin{pmatrix} s_{\mathrm{h}} & s_{\mathrm{hk}} & 0 \\ 0 & -s_{\mathrm{hk}} & s_{\mathrm{k}} \end{pmatrix}\begin{pmatrix} r_{\mathrm{h}} - 1/2 \\ r_{\mathrm{hk}} - 1/2 \\ r_{\mathrm{k}} - 1/2 \end{pmatrix} \quad \text{(x12)}$$

Eq. (x12) can be changed to Eq. (8).

7. References

1. Verrelst B, Ham RV, Vanderborght B, et al. The pneumatic biped “Lucy” actuated with pleated pneumatic artificial muscles. Auton Robots 2005;18(2):201–213.
2. Hosoda K, Takayama H, Takuma T. Bouncing monopod with bio-mimetic muscular-skeleton system. In: Proceedings of the IEEE/RSJ International Conference on Intelligent Robots and Systems (IROS2008); 2008 Sep 22–26; Nice, France. IEEE; 2008. p. 3083–3088.
3. Niiyama R, Kuniyoshi Y. Design principle based on maximum output force profile for a musculoskeletal robot. Ind Rob. 2010; 37(3):250–255.
4. Niiyama R, Nishikawa S, Kuniyoshi Y. Biomechanical approach to open-loop bipedal running with a musculoskeletal athlete robot. Adv Rob. 2012;26(2–3):383–398.
5. Nakanishi Y, Mizuuchi I, Yoshikai T, et al. Pedaling by a redundant musculo-skeletal humanoid robot. In: Proceedings of 5th IEEE-RAS International Conference on Humanoid Robots (Humanoids2005); 2005 Dec 5; Tsukuba, Japan. IEEE; 2005. p. 606–611.
6. Bernstein NA. The coordination and regulation of movements. New York (NY): Oxford, Pergamon Press; 1967.
7. Torres-Oviedo G, Ting LH. Muscle synergies characterizing human postural responses. J Neurophysiol. 2007;98(4):2144–2156.
8. Chvatal SA, Ting LH. Common muscle synergies for balance and walking. Front Comput Neurosci. 2013;7(48).
9. Cappellini G, Ivanenko YP, Poppele RE, et al. Motor patterns in human walking and running. J Neurophysiol. 2006;95(6):3426–3437.
10. Marchis CD, Castronovo AM, Bibbo D, et al. Muscle synergies are consistent when pedaling under different biomechanical demands. In: Proceedings of Annual International Conference of the IEEE Engineering in Medicine and Biology Society; 2012 Aug 28–Sep 1; San Diego, CA, USA. IEEE; 2012. p. 3308–3311.
11. Hug F, Turpin N, Guevel A, et al. Is interindividual variability of EMG patterns in trained cyclists related to different muscle synergies? J Appl Phys. 2010;108(6):1727–1736.

12. Hug F, Turpin N, Couturier A, et al. Consistency of muscle synergies during pedaling across different mechanical constraints. J Neurophysiol. 2011;106(1):91–103, 2011.
13. Artemiadis PK,. Kyriakopoulos KJ. EMG-based teleoperation of a robot arm in planar catching movements using ARMAX model and trajectory monitoring techniques. In: Proceedings of IEEE International Conference on Robotics and Automation; 2006 May 15–19; Orlando, FL, USA. IEEE; 2006. p. 3244–3249.
14. Ajoudani A, Godfrey SB, Catalano M, et al. "Teleimpedance control of a synergy-driven anthropomorphic hand. In: Proceedings of IEEE/RSJ International Conference on Intelligent Robots and Systems; 2013 Nov 3–7; Tokyo, Japan. IEEE; 2014. p. 1985–1991.
15. Ison M, Vujaklija I, Whitsell B, et al. Simultaneous myoelectric control of a robot arm using muscle synergy-inspired inputs from high-density electrode grids. In: Proceedings of IEEE International Conference on Robotics and Automation; 2015 May 26–30; Seattle, WA, USA. IEEE; 2015. p. 6469–6474.
16. Cimolato A, Piovanelli E, Bortoletto R. Muscle synergies for reliable NAO arm motion control: an online simulation with real-time constraints. In: Proceedings of IEEE International Conference on Simulation, Modeling, and Programming for Autonomous Robots; 2016 Dec 13–16; San Francisco, CA, USA. IEEE; 2017. p. 191–196.
17. Lunardini F, Casellato C, d'Avella A, et al. Robustness and reliability of synergy-based myocontrol of a multiple degree of freedom robotic arm. IEEE Trans Neural Syst Rehabil Eng. 2016;24(9):940–950.
18. Cunha T, Vieira PM, Costa K, et al. "Looking for motor synergies in Darwin-OP biped robot. In: Proceedings of IEEE International Conference on Robotics and Automation; 2016 May 16–21; Stockholm, Sweden. IEEE; 2016. p. 1776–1781.
19. Raasch CC, Zajac FE. Locomotor strategy for pedaling: Muscle groups and biomechanical functions. J Neurophysiol. 1999;82(2):515–525.
20. Ting LH, Kautz SA, Brown DA, et al. Phase reversal of biomechanical functions and muscle activity in backward pedalling. J Neurophysiol. 1999;81(2):544–551.
21. Neptune RR, Kautz SA, Zajac FE. Muscle contributions to specific biomechanical functions do not change in forward versus backward pedalling. J Biomech. 2000;33(2):155–164.
22. AIST Human Body Database [Internet]. Tokyo:AIST; 2011.

Available from: https://www.dh.aist.go.jp/database/properties/index-e.html

23. Ariga Y, Pham H, Uemura M, et al. Novel equilibrium-point control of agonist-antagonist system with pneumatic artificial muscles. In: Proceedings of IEEE International Conference on Robotics and Automation; 2012 May 14–18; Saint Paul, MN, USA. IEEE; 2012. p. 1470–1475.
24. Hirai H, Pham H, Ariga Y, et al. Cognitive Neuroscience Robotics A. Tokyo: Springer; 2016. Motor control based on the muscle synergy hypothesis; p. 25-50.
25. Hirai H, Miyazaki F, Naritomi H, et al. On the origin of muscle synergies: Invariant balance in the co-activation of agonist and antagonist muscle pairs. Front Bioeng Biotechnol. 2015;3:192.

Table titles

Table I. Robot body parameters

Table II. Definition and function of the agonist–antagonist (A-A) ratio and agonist–antagonist (A-A) sum.

Table I. Robot body parameters

	Segment	***Length*** [cm]	***Mass*** [kg]	***Position of centre of mass*** [cm]
Robot	Thigh	39.0	2.40	18.5 (from upper side)
	Shank	36.0	1.24	14.6 (from upper side)
	Foot	18.0	0.31	10.7 (from toe)
Human	Thigh	41.0	5.05	19.4 (from upper side)
	Shank	38.0	2.62	15.4(from upper side)
	Foot	22.0	0.76 (Estimated)	13.8 (from toe) (Estimated)

Table II. Definition and function of the agonist–antagonist (A-A) ratio and agonist–antagonist (A-A) sum.

Label	***Definition***	***Function***
s_{h}	$m_{\mathrm{h,Ext}} + m_{\mathrm{h,Flex}}$	Hip joint stiffness increment
s_{hk}	$m_{\mathrm{hk,Ext}} + m_{\mathrm{hk,Flex}}$	Hip and knee joint stiffness increment
s_{k}	$m_{\mathrm{k,Ext}} + m_{\mathrm{k,Flex}}$	Knee joint stiffness increment
s_{a}	$m_{\mathrm{a,Ext}} + m_{\mathrm{a,Flex}}$	Ankle joint stiffness increment
r_{h}	$m_{\mathrm{h.Ext}}/(m_{\mathrm{h.Ext}} + m_{\mathrm{h.Flex}})$	Hip-joint angle extension
r_{hk}	$m_{\mathrm{hk.Ext}}/(m_{\mathrm{hk.Ext}}+m_{\mathrm{hk.Flex}})$	Hip and knee joint angle extension
r_{k}	$m_{\mathrm{k.Ext}}/(m_{\mathrm{k.Ext}}+m_{\mathrm{k.Flex}})$	Knee joint angle extension
r_{a}	$m_{\mathrm{a.Ext}}/(m_{\mathrm{a.Ext}} + m_{\mathrm{a.Flex}})$	Ankle joint angle extension (plantar flexion)

Figure Captions

Figure 1. Procedure of this study.

Figure 2. Anthropomorphic legs. A simple diagram of robot structure is shown on left side. Mass adjustment and length of each segment are shown on right side.

Figure 3. Pneumatic circuit from air pressure source to PAM. (a) JUN-AIR compressor model 12-25, Gast Manufacturing Inc., USA. (b) Custom-made air pressure controller; (b1)IR2020-02G, SMC Corporation, Japan, (b2)VQZ312-5M1-C6, SMC Corporation, Japan, (b3)MPYE-5-1/8-LF-010-B, FESTO AG & Co. KG, Germany. (c) Musculoskeletal robot; (c1) TSND121, ATR-Promotions, Japan, (c2) Φ2.54 cm PAM, Kanda Tsushin Kogyo, Japan.

Figure 4. Customized bicycle. This device consists of city-cycle style bicycle, extra chain, extra sprocket, and electromagnetic brake.

Figure 5. Lower limb musculoskeletal model. (a) muscle configuration; (b) joint and kinematic configuration.

Figure 6. One-to-one correspondence of biomechanical functions between simulation-based analysis and EP-based synergies. In ankle translation, the direction of [Ext/Flex] and [Ant/Post] correspond to $[\mathbf{u}_R, \Delta w_R(t)]$ and $[\mathbf{u}_\phi, \Delta w_R(t)]$, respectively. When the value of $\Delta w_R(t)$ becomes more than or less than zero, the ankle EP becomes [Flex] or [Ext]. When the value of $\Delta w_\phi(t)$ becomes more than or less than zero, the ankle EP becomes [Ant] or [Post]. In ankle rotation, [Plant/Dorsi] corresponds to r_{a}. At a value of r_{a} close to 0 or 1.0, ankle angle becomes [Dorsi] or [Plant].

Figure 7. Process flow diagram for transferring human skill to a musculoskeletal robot. The measured EMG signals of the eight muscles are converted into two functions, i.e. EP-based synergy vectors (mechanical impedance) and synergy activation coefficients (virtual trajectory). This conversion simplifies the discussion of the motor strategy and implementation to robot.

Figure 8. Experimental setup. EMG activity and kinematics were collected from a subject pedalling the crank on the customized bicycle with the electromagnetic brake.

Figure 9. EP-based synergies of ankle translation [Ext/Flex], [Ant/Post] and ankle rotation [Plant/Dorsi]. Upper and lower parts show forward and backward pedalling, respectively. In ankle translation, RGB bar graphs express EP-based synergy vectors and orange dots-and-line graphs show synergy activation coefficients. In ankle rotation, A-A ratios of ankle are shown as equilibrium angle of ankle joint.

Figure 10. Comparison of total pedalling force and corresponding directional vector for the musculoskeletal robot and the five human subjects. The direction and magnitude of pedalling force are shown by orange and yellow arrows (directional vector plot).

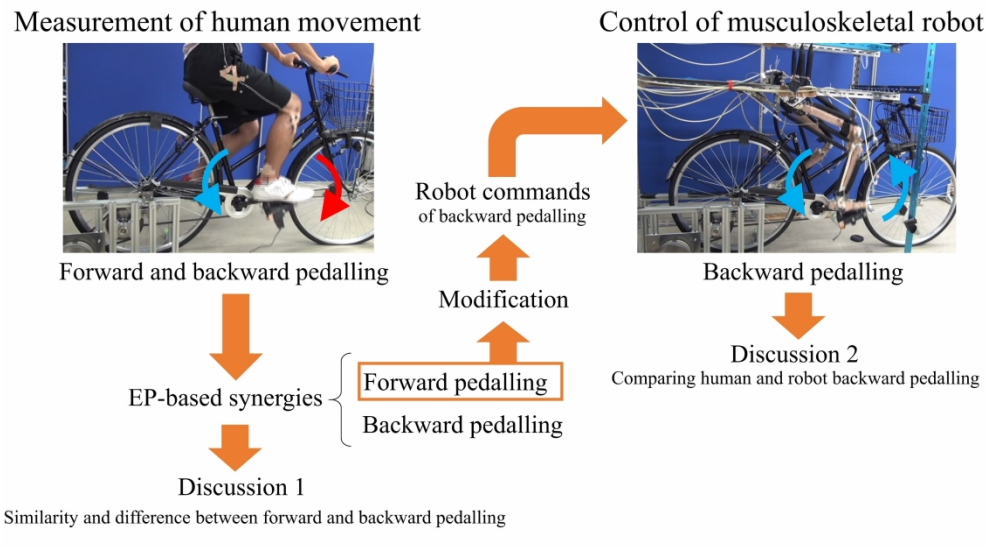

Figure 1. Procedure of this study.

130x73mm (600 x 600 DPI)

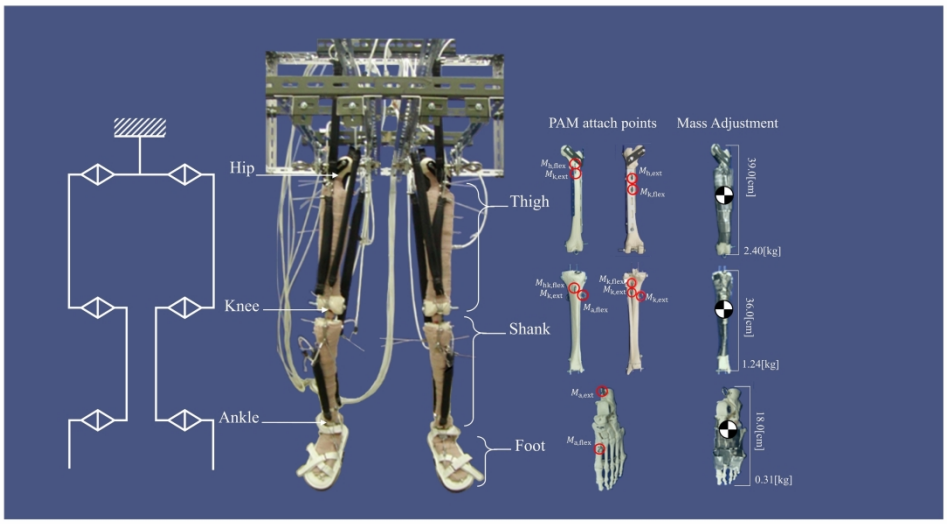

Figure 2. Anthropomorphic legs. A simple diagram of robot structure is shown on left side. Mass adjustment and length of each segment are shown on right side.

130x73mm (600 x 600 DPI)

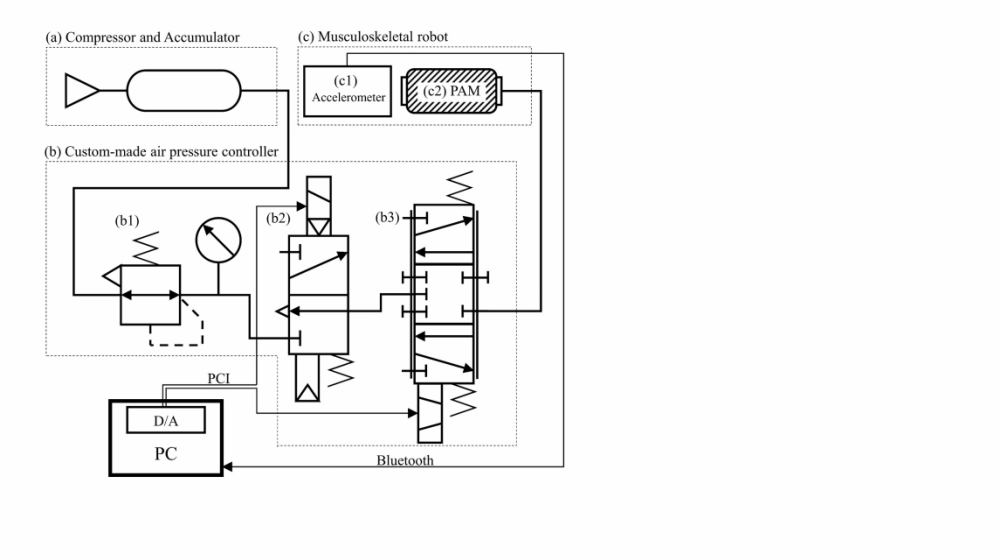

Figure 3. Pneumatic circuit from air pressure source to PAM. (a) JUN-AIR compressor model 12-25, Gast Manufacturing Inc., USA. (b) Custom-made air pressure controller; (b1)IR2020-02G, SMC Corporation, Japan, (b2)VQZ312-5M1-C6, SMC Corporation, Japan, (b3)MPYE-5-1/8-LF-010-B, FESTO AG & Co. KG, Germany. (c) Musculoskeletal robot; (c1) TSND121, ATR-Promotions, Japan, (c2) Φ2.54 cm PAM, Kanda Tsushin Kogyo, Japan.

130x73mm (600 x 600 DPI)

Figure 4. Customized bicycle. This device consists of city-cycle style bicycle, extra chain, extra sprocket, and electromagnetic brake.

130x73mm (600 x 600 DPI)

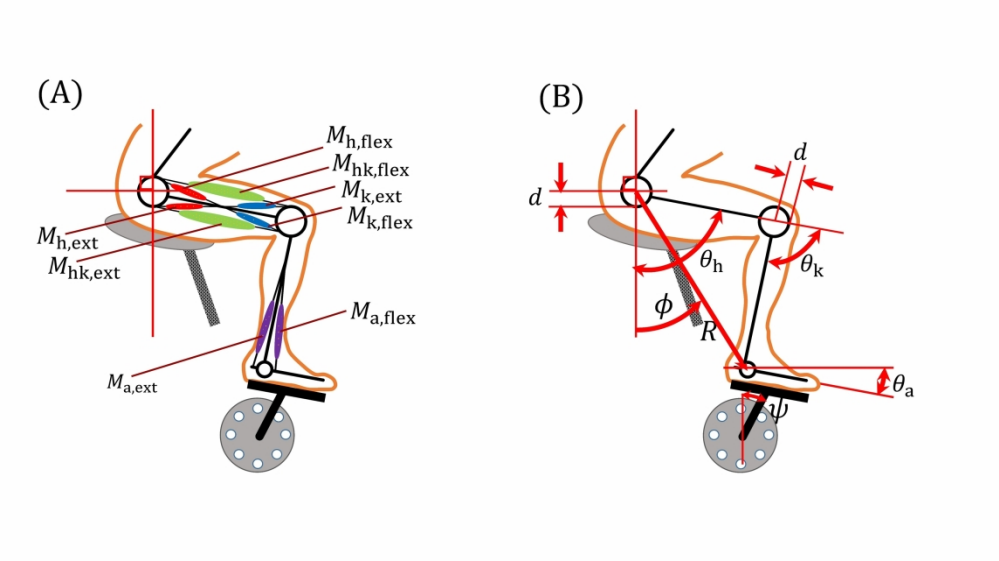

Figure 5. Lower limb musculoskeletal model. (a) muscle configuration; (b) joint and kinematic configuration.

130x73mm (600 x 600 DPI)

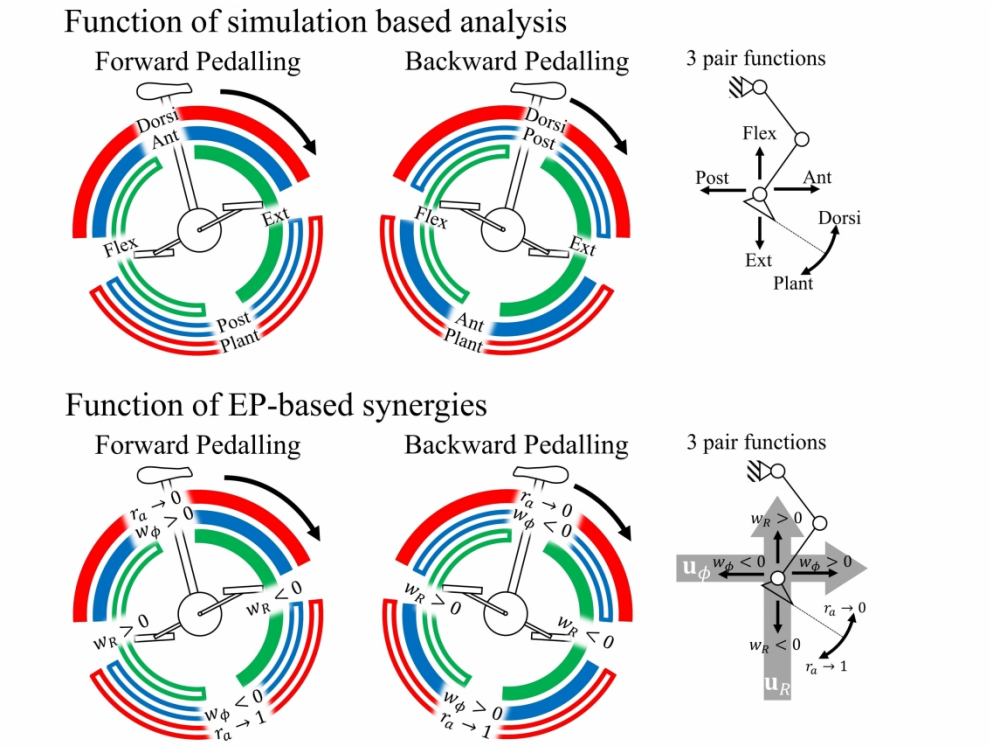

Figure 6. One-to-one correspondence of biomechanical functions between simulation-based analysis and EP-based synergies. In ankle translation, the direction of [Ext/Flex] and [Ant/Post] correspond to [u_R, 〖Δw〗_R (t)] and [u_ϕ, 〖Δw〗_R (t)], respectively. When the value of 〖Δw〗_R (t) becomes more than or less than zero, the ankle EP becomes [Flex] or [Ext]. When the value of 〖Δw〗_ϕ (t) becomes more than or less than zero, the ankle EP becomes [Ant] or [Post]. In ankle rotation, [Plant/Dorsi] corresponds to r_a. At a value of r_a close to 0 or 1.0, ankle angle becomes [Dorsi] or [Plant].

112x84mm (600 x 600 DPI)

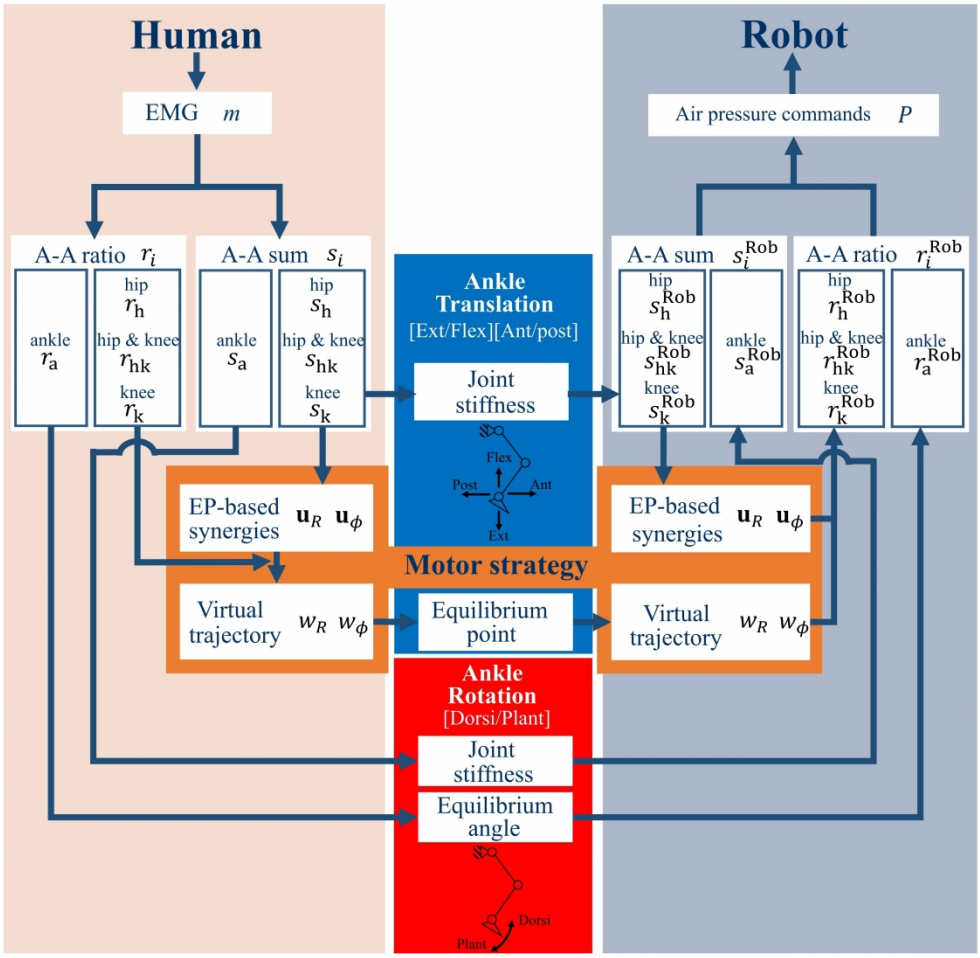

Figure 7. Process flow diagram for transferring human skill to a musculoskeletal robot. The measured EMG signals of the eight muscles are converted into two functions, i.e. EP-based synergy vectors (mechanical impedance) and synergy activation coefficients (virtual trajectory). This conversion simplifies the discussion of the motor strategy and implementation to robot.

172x177mm (600 x 600 DPI)

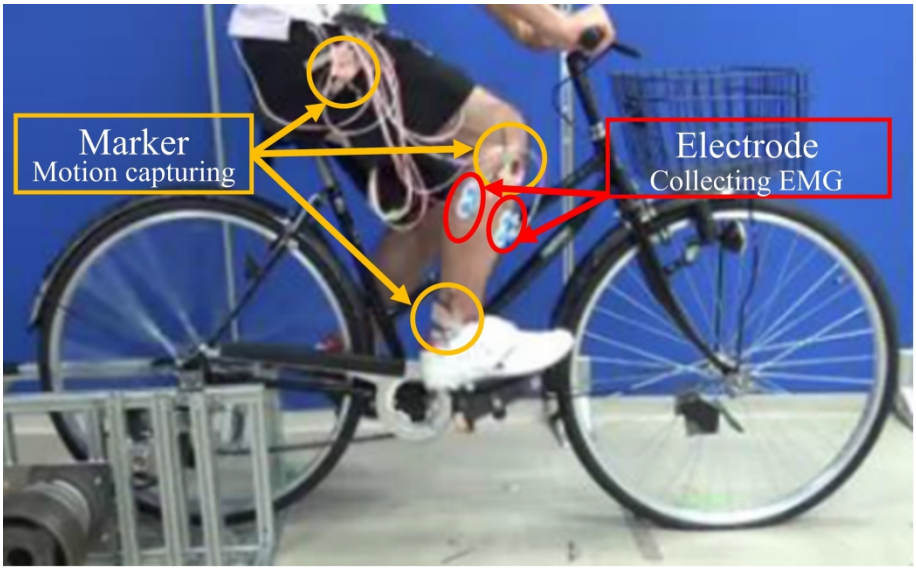

Figure 8. Experimental setup. EMG activity and kinematics were collected from a subject pedalling the crank on the customized bicycle with the electromagnetic brake.

130x73mm (600 x 600 DPI)

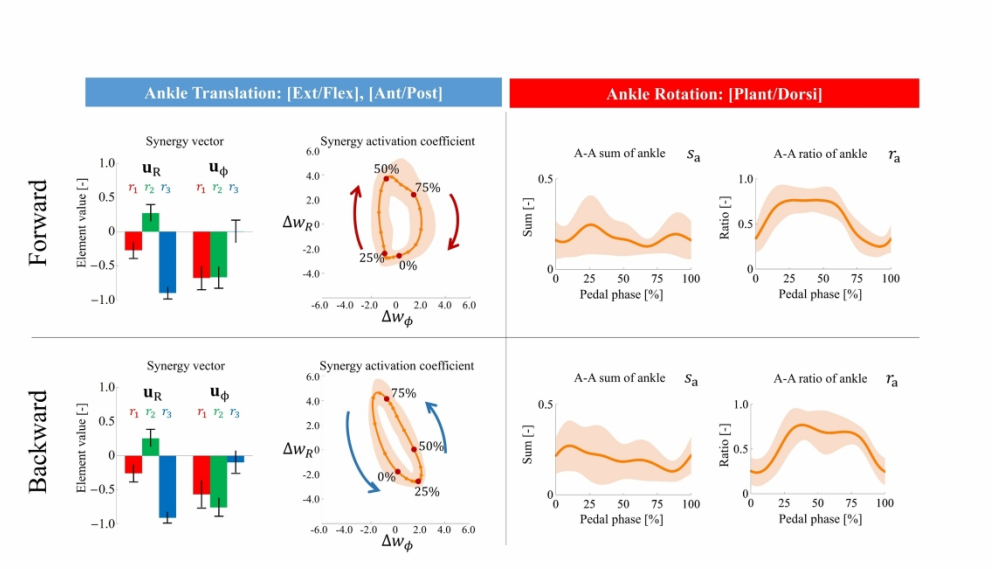

Figure 9. EP-based synergies of ankle translation [Ext/Flex], [Ant/Post] and ankle rotation [Plant/Dorsi]. Upper and lower parts show forward and backward pedalling, respectively. In ankle translation, RGB bar graphs express EP-based synergy vectors and orange dots-and-line graphs show synergy activation coefficients. In ankle rotation, A-A ratios of ankle are shown as equilibrium angle of ankle joint.

128x74mm (600 x 600 DPI)

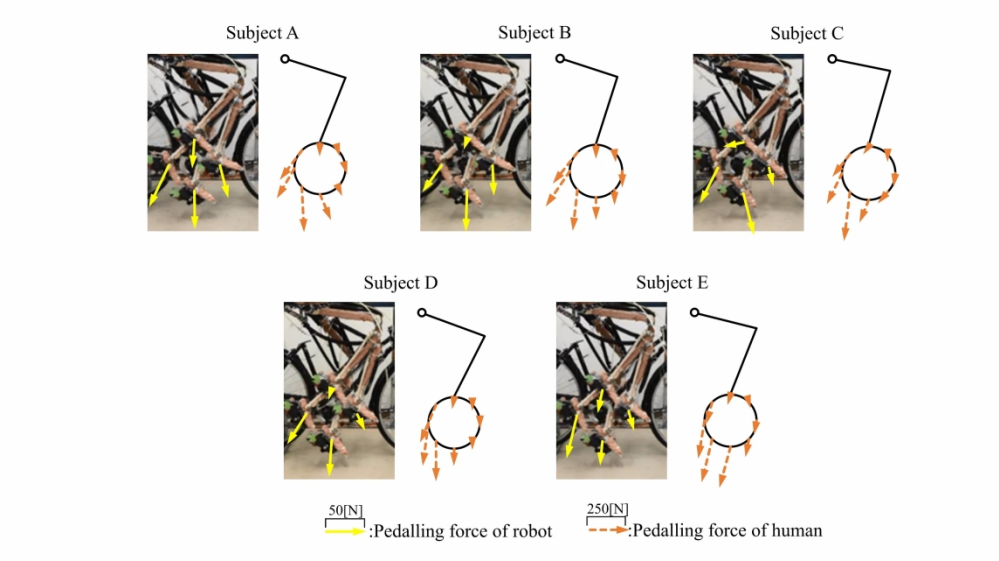

Figure 10. Comparison of total pedalling force and corresponding directional vector for the musculoskeletal robot and the five human subjects. The direction and magnitude of pedalling force are shown by orange and yellow arrows (directional vector plot).

130x73mm (600 x 600 DPI)